Applied Thermal Engineering 161 (2019) 114180

Contents lists available at ScienceDirect

Applied Thermal Engineering

journal homepage: www.elsevier.com/locate/apthermeng

Research Paper

Thermosyphon bushing: design, simulation and implementation

Chunmeng Xu*, Lukas Graber

Georgia Institute of Technology, School of Electrical and Computer Engineering, Atlanta, GA 30332, USA

HIGHLIGHTS

- This paper presents a new application of thermosyphons in electrical equipment.
- Thermosyphon bushing's performances have been validated by experiments and models.
- A thermal network model has been developed for thermosyphon bushings.
- Effective thermal conductivities of thermosyphon bushings could be estimated.
- The prototypes have been built and tested for a vacuum-insulated disconnect switch.

ARTICLE INFO

Keywords:
Thermosyphon
Bushing
Vacuum switchgear
Thermal network model

ABSTRACT

In order to improve the electric current rating of a vacuum-insulated disconnect switch, a copper-water thermosyphon has been embedded into an electrical bushing to achieve significantly higher effective thermal conductivity and lower hotspot temperatures of the bushing. The temperature profiles of a thermosyphon bushing conductor under different heat loads and filling ratios have been characterized by experiments. For the purpose of estimating the performances of any thermosyphon bushing with various dimensions, working fluids and filling ratios, a thermal network model with lumped thermal capacitors has been established. Characteristic features of thermosyphon bushings like the thick pipe walls and the distributed Joule heat sources are represented in the model. This model successfully predicted the effective thermal conductivity and hotspot temperatures of a thermosyphon bushing prototype designed for a vacuum-insulated disconnect switch. Because of the compact designs of thermosyphon bushings, they can be implemented in a wide range of power equipment, such as vacuum switchgear, disconnect switches, plasma chambers, and high-power physics experiments.

1. Introduction

1.1. Problem statement

Electrical bushings are devices that provide insulated paths for the electric current passing through a wall or an equipment enclosure. Bushings generally have slim and long bodies with metal conductors as the core and electrical insulation structures surrounding the metal conductors. When the electric current flows through a bushing, Joule heating will be generated along the metal conductor, which causes hotspots in the insulation layers if the heat is not properly dissipated [1,2].

The slim and long bodies of bushings will also bring problems if the bushing needs to conduct heat from one end (usually within the equipment enclosure) to the other end (usually outside the equipment enclosure). For example, in a vacuum-insulated disconnect switch whose switch is enclosed inside a vacuum chamber, the bushings provide the only electrically and thermally conductive path from the switch-in-chamber to the outside. Therefore, the Joule heat generated within the vacuum chamber could only be dissipated conductively through the bushings, as the convective heat transfer is attenuated inside the vacuum chamber and hotspot temperatures in the switch are too low to transfer heat through radiation. As the Joule heating is proportional to the square of electric current, with restricted heat dissipation capabilities of the bushings, the electric current rating of this disconnect switch could not be upscaled. In our effort to increase the continuous current rating of this vacuum-insulated disconnect switch from 100 A to 600 A, the heat transfer capability of the bushings is the bottleneck that should be tackled.

Traditionally, the high-voltage bushings are cooled by oil circulations within their insulation structures. This method does not apply to our disconnect switch because the bushings do not have enough

* Corresponding author.
E-mail address: chunmengxu@gatech.edu (C. Xu).

https://doi.org/10.1016/j.applthermaleng.2019.114180
Received 30 November 2018; Received in revised form 23 July 2019; Accepted 24 July 2019
Available online 24 July 2019
1359-4311/

Nomenclature

A	cross section area (m^2)
c_p	heat capacity at constant pressure (J/(kg·K))
FR	filling ratio compared to evaporator volume
g	gravitational acceleration (m/s^2)
h_{fg}	latent heat of vaporization (J/kg)
k	thermal conductivity (W/(m·K))
l	length (m)
P	pressure (Pa)
Q	heat flow (W)
q	heat flux (W/m^2)
R	electrical resistance (Ω)
R_T	thermal resistance (K/W)
T_{ref}	reference temperature, 293.15 K
TB	thermosyphon Bushing
V	volume (m^3)
w	thickness (m)

Greek symbols

α	thermal diffusivity (m^2/s)
α_R	temperature coefficient of electrical resistance (1/K)
β	constant coefficient in Eq. (3)
γ	linear coefficient of temperature in Eq. (3)
μ	dynamic viscosity (Pa·s)
ρ	density (kg/m^3)

Subscripts

A	adiabatic section
atm	atmosphere
c	condenser section
$conv$	convection
e	evaporator section
f	liquid state of working fluid
i	inner surface
out	pipe-atmosphere interface at condenser
s	vapor space
sat	saturation
TB	overall thermosyphon bushing
v	vapor state of working fluid

insulation layers to contain the oil. However, the cooling liquid could be contained within the bushing's metal conductor. This solution would be very compact, clean, compatible with vacuum and applicable in all dry-type insulated bushings. As this metal-fluid combination works like a heat pipe with regards to heat transfer processes, the overall device could be called as heat pipe bushing. In our application, we call this product as thermosyphon bushing (TB) because the bushings are vertically installed and there is not a wick inside the metal conductor chamber.

1.2. Literature review

The idea of incorporating a heat pipe in an electrical bushing has been proposed in literature: Zhang [3] and Birgerson [4] have respectively filed patents for structures combining heat pipes and electrical bushings in transformer applications. Zeng [5] was the first one to call his setup as "thermal siphon bushing" in a paper published in 2000. Zeng [5] put water into the hollow copper conductor of a 350 kV BIL 1200 A paper-resin bushing, and this thermal siphon bushing could pass 1800 A heat-run test. That is, the electric current carrying capability of the bushing was increased by 50% in thermosyphon state. Zeng [5] also tried to find the critical current of this thermal siphon bushing through simple calculations, but there were not sufficient presentations of calculated results in the paper.

In 2002, Yamano et al. [6] inserted a heat pipe into the electrode of a vacuum interrupter to reduce the temperature rise at the contact area. The results showed that the contact temperature in a heat pipe installed case was 130 °C after 2000 A conducted for 120 min, while the same contact temperature hit 185 °C without a heat pipe. Temperature profiles were given to demonstrate this achievement.

Yu et al. [7] also applied a gravity heat pipe (bushing) into a 126 kV 2000 A vacuum interrupter for reduced hotspot temperatures. As the thermal resistance of the heat pipe (bushing) was around 30% of that of a pure copper conductor, the temperature of contact area was simulated to be 67 °C lower by incorporating the heat pipe (bushing).

However, even though most of the studies provided complete temperature profiles to demonstrate the outstanding thermal performances of TBs, there is not a detailed discussion on the theoretical work like why a TB is different from a traditional thermosyphon, and how to estimate the potential performances of TBs through modelling. More characterizations are also needed to define the structure, working principles and applicable ranges of a TB in order to get this thermally-optimized device more implementations into power systems.

1.3. Contributions

This work presents introductory discussions on TBs from both experimental and modelling perspectives. A TB conductor test rig was first built to study its basic performances under different heat load inputs and filling ratios. A lumped element thermal network model that was originally built for thermosyphons has been improved to describe TBs. The characteristic features of TBs such as distributed Joule heat sources and thick pipe walls are included to better estimate the range of hotspot temperatures and the equivalent thermal conductivity of a TB. The operational limits of the TB can also be assessed with modelled results. At last, a 15 kV-rated TB prototype has been designed, manufactured and tested for our vacuum-insulated disconnect switch application. The performances of this TB prototype meet the estimates of our thermal network model, which also demonstrates the thermal network model's validity.

2. Experimental approach

2.1. Test setup

For illustration, a schematic diagram of the TBs and the test setup of TB conductor experiments are shown in Fig. 1. The TB's pipe wall material was chosen to be copper due to its excellent electrical conductivity, the TB's working fluid was chosen to be water due to its high density, high surface tension, high latent heat, low viscosity and suitable boiling temperature. Different from a typical thermosyphon whose copper wall thickness is minimized, a TB needs substantial cross-sectional area of pipe wall for better electric current conduction performances.

The physical parameters of the TB conductor are shown in Table 1. In the setup, a Magna-Power TSA5-900/208 power supply provided constant DC current through the TB and four parallel-connected 1 Ω heating resistors at the same time. The resistors in evaporator section were heat sources that represented the heat loads from vacuum-insulated disconnect switch. Joule heating also existed within TB's pipe walls due to the flowing electric current. The evaporator and adiabatic sections were packed inside the thermal insulation foam in the TB

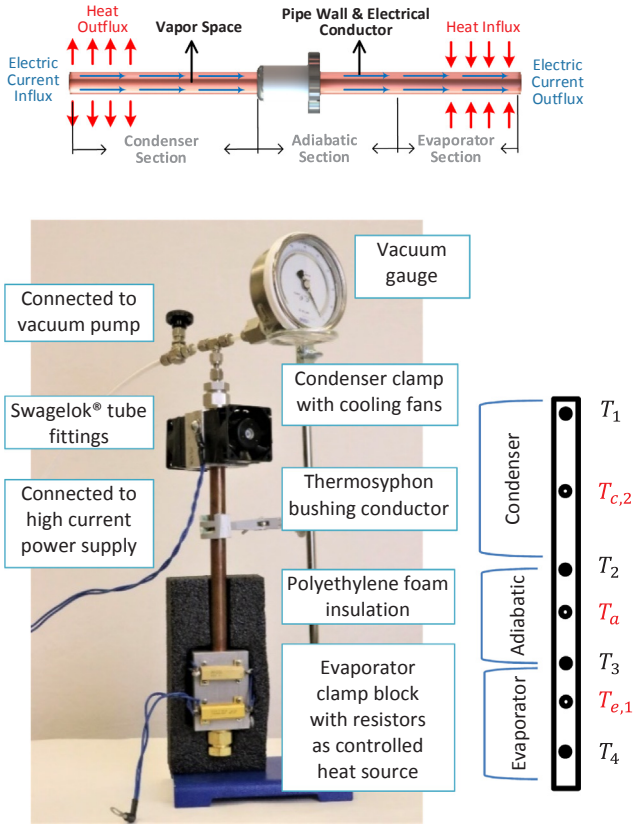

Fig. 1. Thermosyphon bushing (TB) structure and TB conductor test setup with thermocouple locations for temperature readings.

Table 1
Dimensions of TB conductor and TB prototype.

Properties	Parameters
Total length	0.40 m (conductor), 0.50 m (prototype)
Evaporator length	0.09 m
Condenser length	0.18 m (conductor), 0.13 m(prototype)
Inner diameter	1.27 cm
Outer diameter	1.90 cm (conductor), 2.54 cm (prototype)

conductor test. At the condenser section, forced air convection cooling was achieved by two DC fans providing airflows up to 64 m^3/h. Aluminum blocks were attached at both evaporator and condenser of the TB conductor to minimize contact resistance between the TB cylindrical wall and the heat source (resistors) or sink (fans). The internal vacuum of the TB was achieved by a vacuum scroll pump and the pressure was monitored by a vacuum gauge. By changing the electric current flowing through the TB, the heat load inputs ranged from 20 W to 100 W (or 150 W under high filling ratios). The actual amount of power generated in the heating resistors and the pipe wall were measured by a voltmeter.

The temperatures were measured at the bottom of the evaporator (T_4), the interface between evaporator and adiabatic section (T_3), the interface between adiabatic and condenser section (T_2), and the top of condenser section (T_1) as shown in Fig. 1. Temperatures in TB conductor experiments were obtained by type-K thermocouples attached onto the surface of TB walls. Data was collected at intervals of 1 s and the temperature reading resolution was 0.1 °C.

In this study, the Filling Ratio (FR) is defined as the working fluid volume over the evaporator volume. In order to locate the optimal working conditions of TBs, apparent filling ratios of 10%, 30%, 60%, 90%, 100% and 120% were tested in the TB conductor experiment.

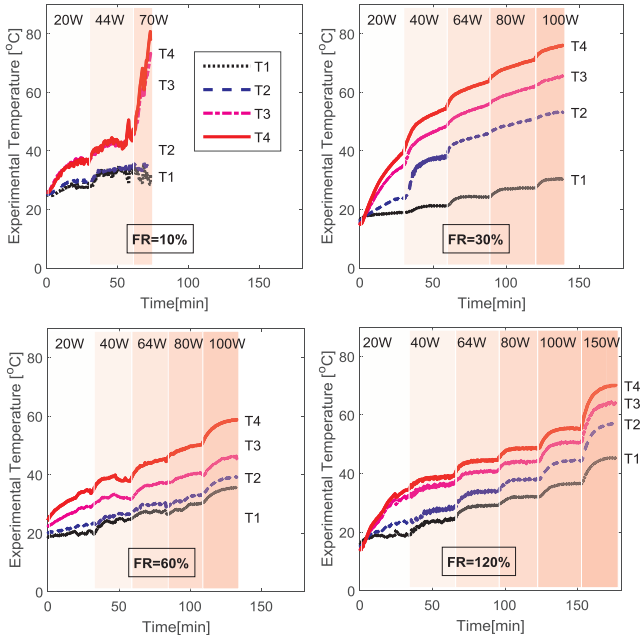

Fig. 2. Temperature profiles in TB conductor experiments under 10%, 30%, 60% and 120% filling ratios.

2.2. Experimental results

Fig. 2 shows the temperature profiles of four tests with TB conductor under 10%, 30%, 60% and 120% filling ratios respectively. The heat load inputs at evaporator ranged from 20 W to 150 W as illustrated by different shades in Fig. 2. The tests usually started from equilibrium at ambient temperature, kept constant heat input for a certain period of time (usually 30 min), then moved to the next heat load input without resetting.

The temperature profiles differ noticeably from FR = 10% test to FR = 120% test. There was an abrupt overheating at evaporator in FR = 10% test under 70 W heat load, which directly pulled the evaporator temperature (T_4) up to 80 °C. It might be the dryout phenomenon that caused this temperature rise, a detailed analysis on operational limits of the TB conductor will be presented in Section 3.2.

In FR = 30% test, the temperatures at locations other than the condenser kept rising continuously. While in FR = 120% test, there were flattened tops of "staircases" which indicated the steady state operations had been achieved. FR = 60% test had a mixed profile of these two patterns, with all temperatures kept ramping up at low heat inputs, the TB conductor approached steady state operation at the end of 100 W input test.

More details about TB conductor temperatures under different FRs and heat inputs are shown in Fig. 3. Data selected here are temperature readings after 20 min of constant heat input operations. The error bars indicate the standard deviations of corresponding groups of temperature readings.

Several common trends could be generalized from this figure. First, the FR = 30% test had the highest evaporator temperature, highest adiabatic temperatures, but lowest condenser temperature. Local film dryout at the evaporator might cause this temperature distribution, so a low filling ratio is not recommended for better thermal performances of TBs. Second, higher FRs could decrease the evaporator temperatures at higher heat inputs. Third, the FR = 120% test had a more uniform temperature distribution throughout the TB, this would lead to a higher effective thermal conductivity (shown in Fig. 4).

The most attractive point of TB is its significantly improved effective thermal conductivity k_{eff}, which represents a steady-state, conduction-dominated, one dimensional heat transfer throughout TB as shown in

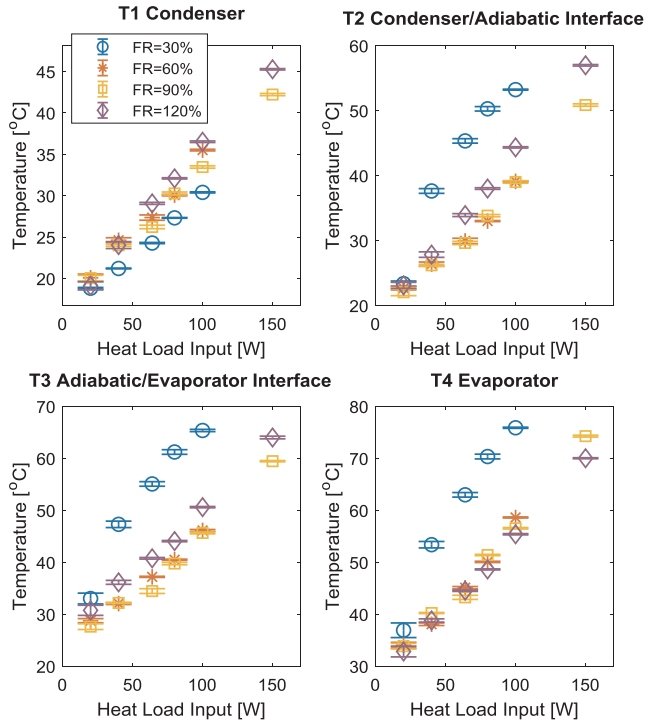

Fig. 3. Steady-state and semi steady temperature readings in TB conductor experiments under various FRs and heat load inputs.

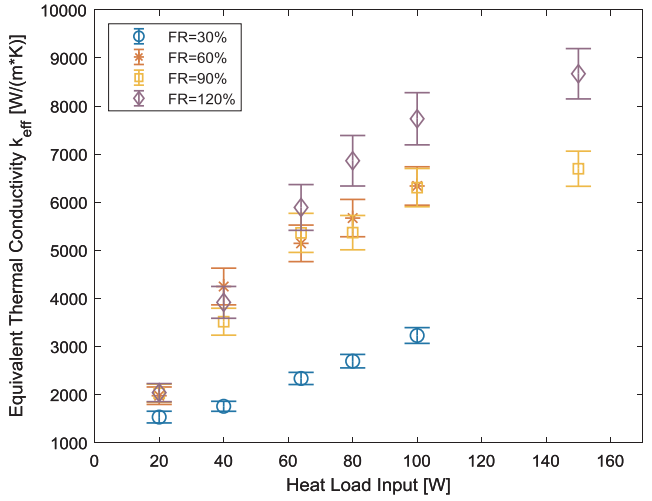

Fig. 4. Calculated equivalent thermal conductivities of TB conductor at different FRs and heat load inputs.

Eq. (1). In the TB conductor, Q is the total heat input containing heat influx at evaporator and distributed Joule loss throughout the TB.

$$k_{eff} = \frac{l_{TB}}{A_{TB}}\frac{Q}{\Delta T} = \frac{l_{TB}}{A_{TB}}\frac{Q}{T_e - T_c} \tag{1}$$

Fig. 4 shows correlations between k_{eff} and input heat loads or FRs based on TB conductor experiments. The error bars of Fig. 4 represent the root sum square uncertainty of k_{eff} derived through propagation of uncertainty law. There was an obviously positive relationship between k_{eff} and input heat loads, but the relationship between k_{eff} and FRs was not clear. k_{eff} improved significantly from 30% FR to 60% FR, and from 90% FR to 120% FR, but stayed rather close between 60% FR and 90% FR.

However, high filling ratios did not benefit k_{eff} at low heat inputs because of the high heat capacity of increased water volume. To balance the performances at both high and low heat loads, a filling ratio between 60% and 90% will be implemented in the TB prototype for vacuum-insulated disconnect switch as described in Section 4. This 60–90% FR is equivalently 13.5–20.25% of total vapor volume, which meets the optimal filling ratio suggested by Imura [8].

The experimental approach is the most reliable way to obtain performances of a TB, but sometimes it is not readily available. Due to the lack of available thick-wall copper tubes in the market, the TB conductor has different wall thicknesses from final TB prototypes for the vacuum disconnect switch as indicated in Table 1. The TB prototypes were manufactured by an electrical bushing company with a rather long leading time. Meanwhile, in order to efficiently predict the performances of final TB prototype, and possibly any TB with different dimensions and working fluids properties, a thermal network model of TB has been developed and trained by TB conductor experimental data.

3. Theoretical analysis

3.1. Thermal network model

The construction of a computational fluid dynamics model is expected to be time-consuming and complicated if only the steady-state effective thermal conductivity k_{eff} and the temperature profiles of TB need to be determined. Comparatively a thermal network model using lumped resistors or capacitors is a more effective approach. Networks built upon combinations of thermal resistors are widely presented in previous literature [9–12], and they have been used to derive the analytical expressions for thermal conductivities of heat pipes [13]. Resistors-based thermal networks are easy to calculate and analyze, but they failed to address the transient performances of heat pipes. Lumped capacitors approach, on the other hand, has been built to study the temperature profiles of heat pipes changing with time [14–17]. Considering the transient processes measured in TB conductor experiments, we choose the lumped capacitors approach to construct the TB's thermal network model.

However, thermal network models built upon traditional heat pipes or thermosyphons could not be directly used in TBs, because TBs have much thicker walls and distributed Joule heat sources along the metal conductor. While traditional thermosyphons use thin-wall pipes and have concentrated heat source at the evaporator. To address these two characteristic features of TBs, we improve the thermal network models with lumped capacitors [14,17] to further explore the steady-state performances of TBs.

Fig. 5 illustrates the heat transfer processes through the thermal network of a TB. The liquid return process has been neglected because of its limited effect on the overall heat transfer [14]. The TB is divided into evaporator, adiabatic and condenser regions vertically with the vapor space interconnects all three regions. Horizontally, it is divided into atmosphere-pipe interface (the aluminum block as evaporator clamp block and condenser clamp block shown in Fig. 1), wall conduction, wall-fluid convection and fluid space. Every region is further divided into two sides to represent the temperature gradients over one region, subscription '1' represents the inflow side boundary and subscription '2' represents the outflow side boundary with shared inner temperature at the middle of one region.

Applying the law of energy conservation to the copper wall conduction regions results in following equations of states:

$$\rho_n V_n c_{p,n}\frac{dT_n}{dt} = Q_{n,1} - Q_{n,2} + Q_{j,n}\ ,\ n = e,\ a,\ c \tag{2}$$

where $Q_{j,n}$ is the Joule heat source. It has a linear relationship with local temperatures as shown in Eq. (3).

$$Q_{j,n} = I^2 R_{T_n} = I^2 R_{ref,n}(1 - \alpha_R T_{ref}) + I^2 R_{ref,n}\alpha_R T_n = \beta_n + \gamma_n T_n\ ,\ n = e,\ a,\ c \tag{3}$$

For the heat conductions through a thick tube wall at evaporator

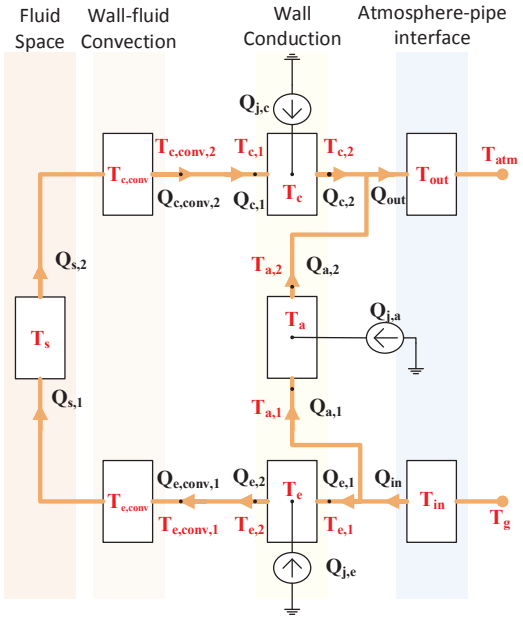

Fig. 5. Thermal network with flows of energy balances in TBs.

and condenser sections of TBs, the Fourier's law can be written as:

$$Q = kA_m\frac{T_i - T_o}{w},\ A_m = \frac{A_o - A_i}{\ln(A_o/A_i)},\ w = r_o - r_i \tag{4}$$

Due to the thickness of TB wall, the cross-sectional area of outer surface differs largely from inner surface, so that the two cross-sectional areas are calculated for each side. Therefore, the input-side heat influx $Q_{n,1}$ and output-side heat outflux $Q_{n,2}$ are expressed as

$$Q_{n,1} = k_nA_{m,n1}\frac{T_{n,1} - T_n}{w_n/2},\ Q_{n,2} = k_nA_{m,n2}\frac{T_n - T_{n,2}}{w_n/2},\ n = e,\ a,\ c \tag{5}$$

Taking Eqs. (3) and (5) into (2), Eq. (2) can be rearranged to

$$\frac{dT_n}{dt} = \left[\frac{\gamma_n}{\rho_nV_nc_{p,n}} - \frac{2\alpha_n}{V_nw_n}(A_{m,n1} + A_{m,n2})\right]T_n + \frac{2\alpha_nA_{m,n1}}{V_nw_n}T_{n,1} + \frac{2\alpha_nA_{m,n2}}{V_nw_n}T_{n,2} + \frac{\beta_n}{\rho_nV_nc_{p,n}} \tag{6}$$

$$\alpha_n = \frac{k_n}{\rho_nc_{p,n}},\ n = e,\ a,\ c$$

Suppose the complicated heat transfers and phase transitions in the fluid space can be represented by a simplified heat conduction process, a first-order differential equation in Eq. (7) can also be derived for the fluid space. For simplicity, we assume a uniform temperature T_s both in the boiling pool and the vapor space, this temperature uniformity normally happens when the working fluid reaches its saturation temperatures.

$$\frac{dT_s}{dt} = \frac{Q_{s,1} - Q_{s,2}}{\rho_sV_sc_{p,s}} = \frac{1}{\rho_sV_sc_{p,s}}\left[\frac{2k_eA_{m,e2}}{w_e}(T_e - T_{e,2}) + \frac{2k_cA_{m,c1}}{w_c}(T_{c,1} - T_c)\right] \tag{7}$$

Eqs. (6) and (7) give four differential equations of temperatures to be solved for, then the basic parameters of TB including k_{eff} can be derived from T_e, T_a, T_c and T_s once obtained. However, there are still intermediate variables like $T_{e,2}$ and $T_{c,1}$ in expressions that should be substituted first. Here, two assumptions are proposed to derive the boundary conditions. First, the algebraic sum of the heat fluxes meeting at a vertex of the thermal network is zero. Second, no temperature gradient exists over the connection lines of the thermal network. Based on these two assumptions, we can derive the following boundary conditions as shown in Eq. (8). Under sufficient cooling conditions, the surface temperature of the condenser clamp at condenser T_{out} equals the atmospheric temperature T_{atm}. The heat transfer coefficient determined by a forced convection cooling is h_{out}, and the surface area for

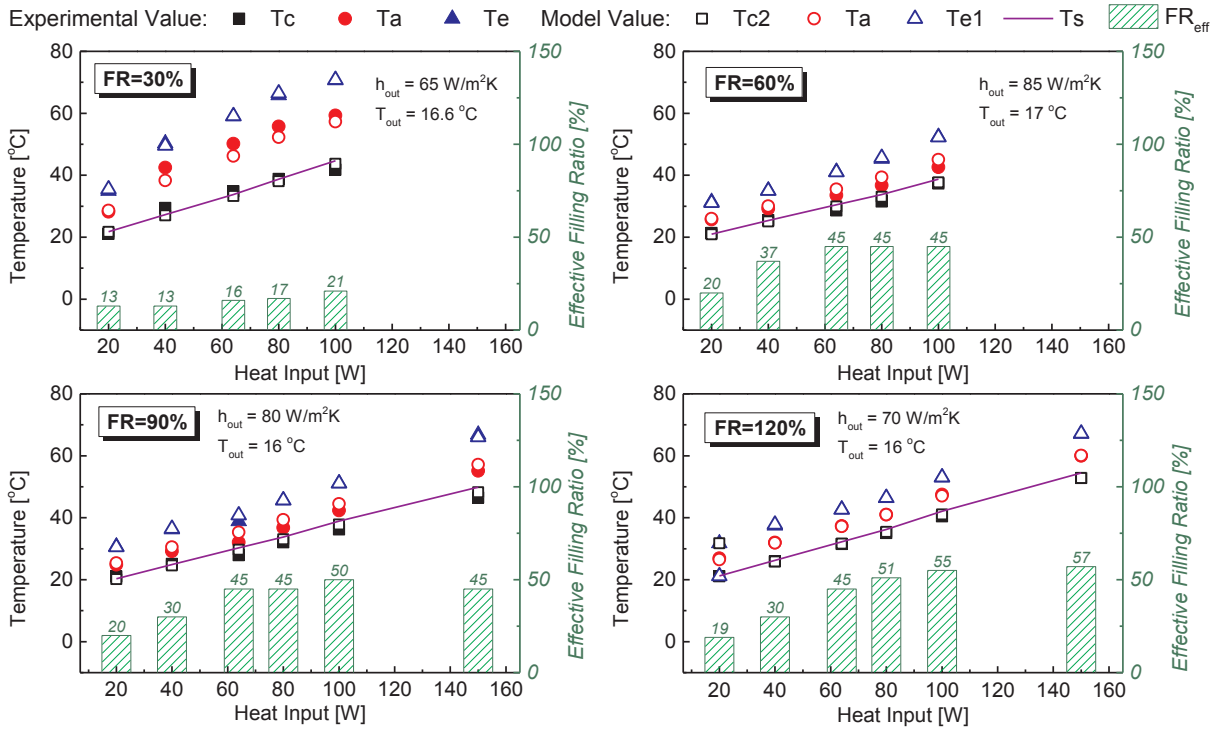

Fig. 6. Comparisons between temperatures from TB conductor experiments and thermal network model. Vapor temperature T_s and effective filling ratios FR_{eff} derived from thermal network model are also included.

dissipation at condenser is A_{out}.

$$T_{e,1} = T_{a,1}\ ,\ Q_{e,1} = Q_{in} - Q_{a,1}\ ,\ T_{e,conv,1} = T_{e,2}$$
$$T_{e,conv} = T_s = T_{c,conv}\ ,\ Q_{e,2} = Q_{e,conv,1}$$
$$T_{c,conv,2} = T_{c,1}\ ,\ Q_{c,conv,2} = Q_{c,1}$$
$$T_{c,2} = T_{a,2}\ ,\ Q_{c,2} + Q_{a,2} = h_{out}A_{out}(T_{c,2} - T_{out}) \quad (8)$$

As for the heat convection processes at the interface of inner pipe wall and working fluid, we assume a nucleate boiling process at the evaporator and a filmwise condensation process at the condenser under normal working conditions. So, the heat transfer coefficient at evaporator h_e is based on Imura's equation [18], while heat transfer coefficient at condenser h_c is based on Nusselt's equation [19]. The effect of different filling ratios is also considered by introducing an effective filling ratio FR_{eff}. This parameter represents the percentage of effective heat transfer area at evaporator after the TB has entered steady or semi stable operations. The thermo-physical properties of water and steam used in Eq. (9) are calculated with equations from [20] and [21].

$$h_e(FR_{eff}\cdot A_{e,i})(T_{e,2} - T_s) = k_e A_{m,e2}\frac{T_e - T_{e,2}}{w_e/2}$$
$$h_e = 0.32\left(\frac{\rho_f^{0.65}k_f^{0.3}c_{p,f}^{0.7}g^{0.2}q^{0.4}}{\rho_v^{0.25}h_{fg}^{0.4}\mu_f^{0.1}}\right)\left(\frac{P_{sat}}{P_{atm}}\right)^{0.3}$$
$$h_c A_{c,i}(T_s - T_{c,1}) = k_c A_{m,c1}\frac{T_{c,1} - T_c}{w_c/2}$$
$$h_c = 0.943\left(\frac{\rho_f k_f^3 g(\rho_f - \rho_v)h_{fg} + 0.68c_{p,f}(T_v - T_c)}{\mu_f L_c(T_v - T_c)}\right)^{0.25} \quad (9)$$

So far, we have derived all boundary conditions to substitute the six intermediate temperature variables by four state temperatures T_e, T_a, T_c and T_s. A detailed list of expressions for the intermediate temperatures is shown below.

$$T_{e,1} = \frac{Q_{in}w_e w_a + 2k_e A_{m,e1}w_a T_e + 2k_a A_{m,a1}w_e T_a}{2k_e A_{m,e1}w_a + 2k_a A_{m,a1}w_e}$$
$$T_{e,2} = \frac{2k_e A_{m,e2}T_e + w_e h_e(FR_{eff}\cdot A_{e,i})T_s}{2k_e A_{m,e2} + w_e h_e(FR_{eff}\cdot A_{e,i})}$$
$$T_{a,1} = T_{e,1}$$
$$T_{a,2} = \frac{2k_c A_{m,c2}w_a T_c + 2k_a A_{m,a2}w_c T_a + h_{out}A_{out}w_a w_c T_{out}}{h_{out}A_{out}w_a w_c + 2k_c A_{m,c2}w_a + 2k_a A_{m,a2}w_c}$$
$$T_{c,1} = \frac{w_c h_c A_{c,i}T_s + 2k_c A_{m,c1}T_c}{2k_c A_{m,c1} + w_c h_c A_{c,i}}$$
$$T_{c,2} = T_{a,2} \quad (10)$$

3.2. Model validation and discussions

Even though most of the model inputs are measurable values like the electric current I, the resistive heating power Q_{in} and the atmospheric temperature T_{atm}, there are empirical inputs that need to be determined with pilot test data. TB conductor test results are thus used to generalize the dissipation heat transfer coefficient h_{out} and effective filling ratio FR_{eff} for the thermal network model. The outer surface temperatures in the model, $T_{e,1}$, T_a and $T_{c,2}$, are correlated with measured temperatures, T_e, T_a, T_c and T_s, through Eq. (11) below.

$$T_{e,1} = \frac{T_4 + T_3}{2}\ ,\ T_a = \frac{T_3 + T_2}{2}\ ,\ T_{c,2} = \frac{T_2 + T_1}{2} \quad (11)$$

As the thermal network model has been built upon the assumption of steady-state operations, temperature values from Fig. 3 are used as references for data fitting with model outputs in order to determine the empirical inputs: h_{out} and FR_{eff}. The best fits of h_{out} and FR_{eff} are shown in Fig. 6 with a comparison of experimental temperatures and simulated temperatures.

The errors between experimental results and theoretical values are below 5% in most cases and below 10% in all cases. Errors mainly exist in adiabatic temperature T_a and condenser temperature T_c, which are probably caused by the assumptions of ideal heat dissipations in the thermal network model: no heat dissipation in the adiabatic section and uniform heat dissipation coefficient in the condenser. In reality, the thermal insulation foam could not prevent all dissipations, and the upper half of the condenser section, which was surrounded by cooling fans, would have larger heat transfer rates than the rest of condenser section. Such differences in the heat transfer coefficient h_{out} at the condenser noticeably affects model results, because h_{out} is a critical parameter that influences both T_c and T_a in the model calculations.

By the assistance of thermal network model, we can also obtain vapor temperature T_s and effective filling ratio FR_{eff} that could not be easily measured in experiments. The effective filling ratio FR_{eff} represents the percentage of effective evaporator area utilized in heat transfer. As shown in Fig. 6, FR_{eff} is only 40–60% of the apparent filling ratio. Considering our TB conductor setup, this reduction was probably caused by the partially flooding in the condenser section.

So far there are two phenomena being attributed to the operational limits: the dryout in FR = 10% test and the reduced FR_{eff} values possibly caused by partial flooding. With the vapor temperature T_s obtained from the thermal network model, we could calculate the maximum heat transfer rate defined by various operational limits, including sonic, flooding, boiling and dryout limits. Using the empirical correlations provided in [9,22], the maximum heat transfer rates Q at different vapor temperatures for the TB conductor are shown in Table 2 below. It can be seen that the sonic limit, flooding limit and boiling limit at high filling ratios are far beyond the heat loads of TB conductor under working conditions. At low filling ratios like FR = 30%, the TB conductor worked at the boundary of boiling limits, so that the evaporator temperature kept rising up as shown in Fig. 2. At even lower filling ratios like FR = 10%, the calculated dryout limit is merely 10 W. Inputting high heat loads like 70 W would certainly lead to abrupt temperature rise at evaporator as shown in Fig. 2. Therefore, low filling ratios in TBs should be avoided for the possible dryout at evaporator.

The significance of this thermal network model is that it provides a shortcut to obtain the estimated temperature profiles of a TB under steady-state conditions, which can easily lead to the calculations of the effective thermal conductivity k_{eff} and operational limits. As discussed in the model descriptions, three out of five input parameters of the thermal network model can be directly measured or assumed: electric current I, heat load Q_{in}, and ambient temperature T_{out}. The heat dissipation coefficient at the condenser h_{out} depends on TB's cooling methods and condenser geometries, this value could be found in numerous handbooks. The only empirical parameter here is the effective filling ratio FR_{eff}. As summarized from TB conductor experiments stated above, the FR_{eff} can be chosen as 40–60% of apparent filling ratios (or initial filling ratios) with slightly higher FR_{eff} at higher heat loads.

4. Thermosyphon bushing application example: In a vacuum-insulated disconnect switch

4.1. Thermosyphon bushing prototype

As indicated in the introduction, a TB prototype has been designed for a vacuum-insulated disconnect switch to improve its continuous current rating from 100 A to 600 A. Different from the TB conductor

Table 2
Calculated heat transfer limits at different vapor temperatures.

T_v	Maximum heat transfer rate Q [W]						
	Sonic	Flooding	Boiling				Dryout
[°C]			FR 30%	FR 60%	FR 90%	FR 120%	FR 10%
20	914	697	58	5026	3723	3009	6
30	1615	826	76	6564	4862	3930	7
40	2736	963	97	8388	6213	5022	9
50	4460	1105	122	10,511	7786	6293	10

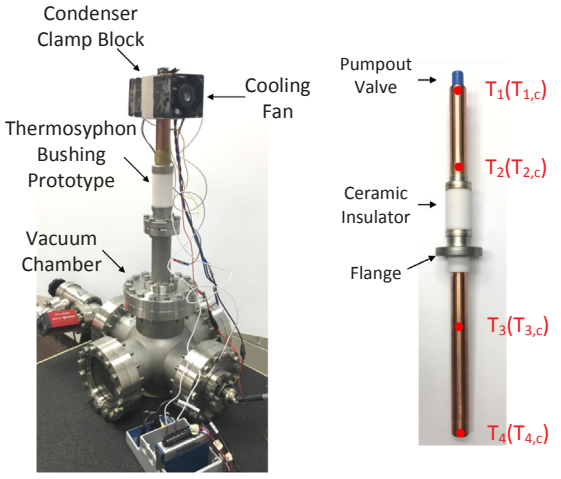

Fig. 7. Test setup of TB prototype and TB prototype structure with RTD sensors locations for temperature measurements.

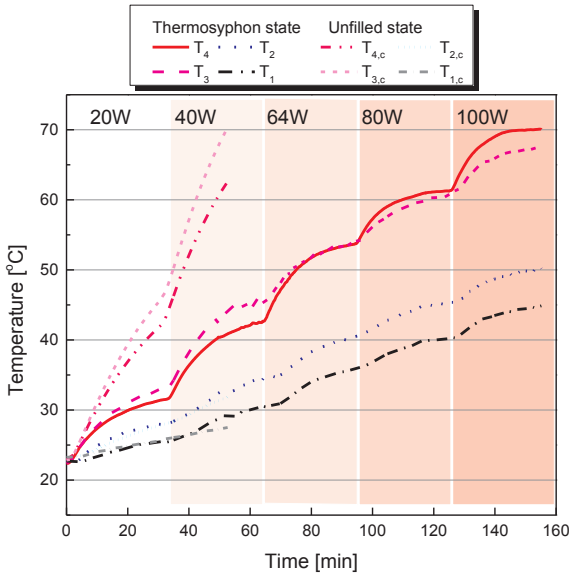

Fig. 8. Temperature profiles of TB prototype tests under unfilled state and thermosyphon state.

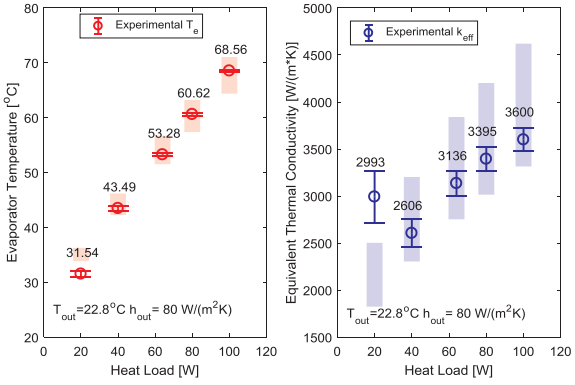

Fig. 9. Comparison between thermal network model defined ranges of values (shades) and values obtained from TB prototype tests (scatters). Error bars of evaporator temperature represent standard deviations, error bars of k_{eff} represent root sum square uncertainty values.

presented in Fig. 1, the TB prototype has a ring ceramic insulator to provide mechanical support and electrical insulation from the vacuum chamber, a knife-edge flange to be mounted onto the vacuum chamber, and a pumpout valve for vacuuming and sealing purposes. The structure of a TB prototype is presented in Fig. 7.

4.2. Thermosyphon bushing prototype test results

In order to resemble the working conditions in the vacuum-insulated disconnect switch, the TB prototype was tested within a six-way cross vacuum chamber following the same procedures described in TB conductor experiments. The test setup of the TB prototype is shown in Fig. 7. The temperatures were obtained from RTD sensors at fine resolution with a time interval of 3 s.

For comparison purposes, the TB prototype was tested in both unfilled state as a pure copper conductor (FR = 0%) and thermosyphon state as a TB (FR = 60%). Fig. 8 clearly shows the advantages of the thermosyphon state: the TB prototype worked in thermosyphon state could transport up to 100 W of heat with highest temperature stabilized to 70 °C, while the TB prototype worked in unfilled state suffered constant temperature rises which went beyond 70 °C at only 40 W heat load. Similar to the results reported in literature [5–7], the heat transfer capability of an electrical bushing has been significantly improved after incorporating a thermosyphon.

The thermal network model built in Section 3 worked effectively in estimating the range of hotspot temperature T_e and effective thermal conductivity k_{eff} of the TB prototype. As shown in Fig. 9, measurements obtained from TB prototype experiments mostly fall into the range defined by the thermal network model using 40–60% effective filling ratio FR_{eff} range. This 40% to 60% FR_{eff} range was generalized from conductor experimental results as stated in Section 3.2. The singularity at 20 W input could be caused by the unstable processes during the test—the hotspot temperature of 32.2 °C had not turned the working fluid into its saturation state. Generally speaking, the thermal network model trained by TB conductor experimental data could successfully estimate the potential performances of TB prototype, which had different physical dimensions and filling ratios from the TB conductor. The validity of our thermal network model is thus demonstrated.

5. Conclusion

Incorporating a thermosyphon into an electrical bushing can significantly improve the bushing's thermal management capabilities, which leads to a higher current rating of corresponding power equipment. This paper takes a medium-voltage, vacuum-insulated disconnect switch as the application of developed TBs, a TB conductor and a TB prototype have been designed, simulated and tested respectively under the working conditions of vacuum-insulated disconnect switch. One of the major novelties of our work is to introduce a thermosyphon-based thermal network model into TB scenarios, adding characteristic features of TBs like thick pipe walls and distributed Joule heat sources to better estimate the temperature distributions along TBs. The effective thermal conductivities, hot spot temperatures and operational limits of TBs could be estimated using this thermal network model, and the validity of model had been confirmed by both TB conductor and TB prototype test results.

The TBs built in this work have shown distinguished thermal management performances. Compared with unfilled state, the TB prototype worked in thermosyphon state could double the heat load transfer rate with the same hot spot temperature, and the maximum effective thermal conductivity achieved is around 8700 W/(m·K) in TB conductor tests and 3600 W/(m·K) in TB prototype tests.

Based on our observations, future work on thermosyphon bushings include visualization studies to identify the dominant mechanisms of thermosyphon bushings, modelling performances of thermosyphon bushings based on conjugate heat transfers, and development of heat

pipe bushings with wicks inside the metal conductors.

In today's fast-evolving power systems with vacuum-insulated power equipment getting more popularity, the TBs could become a key enabling component to improve the continuous current ratings of these vacuum-insulated power equipment, and make them more competitive in meeting the needs of ever-growing electricity consumptions nowadays.

Acknowledgements

The authors would like to thank Tushar Damle from Georgia Institute of Technology for his assistance with setting up the prototype experiment. This work was funded in part by National Science Foundation grant # 1700887.

References

[1] M. Akbari, M. Allahbakhshi, R. Mahmoodian, Heat analysis of the power transformer bushings in the transient and steady states considering the load variations, Appl. Therm. Eng. 121 (2017) 999–1010, https://doi.org/10.1016/j.applthermaleng.2017.05.004.

[2] M. Allahbakhshi, M. Akbari, Heat analysis of the power transformer bushings using the finite element method, Appl. Therm. Eng. 100 (2016) 714–720, https://doi.org/10.1016/j.applthermaleng.2016.02.065.

[3] G. Zhang, W. Niu, X. Wang, W. Xing, Heat pipe type transformer tube, Patent CN101369483, 2011.

[4] J. Birgerson, A. Ravanal, Electrical bushing, Patent EP3007184B1 Patent Appl. EP3007184A1, 2017.

[5] D. Zeng, An experimental thermal siphon bushing, IEEE Trans. Power Deliv. 15 (1) (2000) 175–177, https://doi.org/10.1109/61.847247.

[6] Y. Yamano, S. Kobayashi, M. Matsukawa, Measurements and analysis of temperature rise at electrodes of a vacuum interrupter for high current applications, 20th International Symposium on Discharges and Electrical Insulation in Vacuum, 2002, pp. 419–422, , https://doi.org/10.1109/ISDEIV.2002.1027398.

[7] X. Yu, Z. Liu, Q. Feng, Y. Wei, J. Wang, Research on a gravity heat pipe for high voltage vacuum interrupter, 2008 23rd International Symposium on Discharges and Electrical Insulation in Vacuum, vol. 1, 2008, pp. 129–132, , https://doi.org/10.1109/DEIV.2008.4676736.

[8] H. Imura, K. Sasaguchi, H. Kozai, S. Numata, Critical heat flux in a closed two-phase thermosyphon, Int. J. Heat Mass Transf. 26 (8) (1983) 1181–1188, https://doi.org/10.1016/S0017-9310(83)80172-0.

[9] A. Faghri, Heat Pipe Science and Technology, Global Digital Press, 1995.

[10] D.A. Reay, P. Kew, P.D. Dunn, R. McGlen, Heat Pipes: Theory, Design and Applications, Elsevier Science & Technology, Jordan Hill, United Kingdom, 2006.

[11] C. Ferrandi, F. Iorizzo, M. Mameli, S. Zinna, M. Marengo, Lumped parameter model of sintered heat pipe: transient numerical analysis and validation, Appl. Therm. Eng. 50 (1) (2013) 1280–1290, https://doi.org/10.1016/j.applthermaleng.2012.07.022.

[12] B. Zohuri, Heat Pipe Design and Technology: A Practical Approach, second ed., Springer, Switzerland, 2011, pp. 250–258.

[13] A.B. Solomon, M. Sekar, S.H. Yang, Analytical expression for thermal conductivity of heat pipe, Appl. Therm. Eng. 100 (2016) 462–467, https://doi.org/10.1016/j.applthermaleng.2016.02.042.

[14] B.M. Ziapour, H. Shaker, Heat transfer characteristics of a two-phase closed thermosyphon using different working fluids, Heat Mass Transf. 46 (3) (2010) 307–314, https://doi.org/10.1007/s00231-009-0570-1.

[15] H. Farsi, J.-L. Joly, M. Miscevic, V. Platel, N. Mazet, An experimental and theoretical investigation of the transient behavior of a two-phase closed thermosyphon, Appl. Therm. Eng. 23 (15) (2003) 1895–1912, https://doi.org/10.1016/S1359-4311(03)00147-9.

[16] M. Bernagozzi, S. Charmer, A. Georgoulas, I. Malavasi, N. Michè, M. Marengo, Lumped parameter network simulation of a Loop Heat Pipe for energy management systems in full electric vehicles, Appl. Therm. Eng. 141 (2018) 617–629, https://doi.org/10.1016/j.applthermaleng.2018.06.013.

[17] Z.J. Zuo, A. Faghri, A network thermodynamic analysis of the heat pipe, Int. J. Heat Mass Transf. 41 (11) (1998) 1473–1484, https://doi.org/10.1016/S0017-9310(97)00220-2.

[18] H. Imura, H. Kusuda, J. I. Ogata, T. Miyazaki, N. Sakamoto, Heat transfer in two-phase closed-type thermosyphons, 1979, pp. 712–722.

[19] Y.J. Park, H.K. Kang, C.J. Kim, Heat transfer characteristics of a two-phase closed thermosyphon to the fill charge ratio, Int. J. Heat Mass Transf. 45 (23) (2002) 4655–4661, https://doi.org/10.1016/S0017-9310(02)00169-2.

[20] C.O. Popiel, J. Wojtkowiak, Simple formulas for thermophysical properties of liquid water for heat transfer calculations (from 0°C to 150°C), Heat Transfer Eng. 19 (3) (1998) 87–101, https://doi.org/10.1080/01457639808939929.

[21] Magda Vestfálová, Pavel Šafařík, P. Dančová, M. Veselý, Dependence of the isobaric specific heat capacity of water vapor on the pressure and temperature, EPJ Web Conf. 114 (2016) 02133 http://www.epj-conferences.org/10.1051/epjconf/201611402133https://doi.org/10.1051/epjconf/201611402133.

[22] D. Jafari, A. Franco, S. Filippeschi, P. Di Marco, Two-phase closed thermosyphons: a review of studies and solar applications, Renew. Sustain. Energy Rev. 53 (2016) 575–593, https://doi.org/10.1016/j.rser.2015.09.002.